# Gain functionalized core–shell nanoparticles: The way to selectively compensate absorptive losses

**ARTICLE** *in* JOURNAL OF MATERIALS CHEMISTRY · FEBRUARY 2012

Impact Factor: 7.44 · DOI: 10.1039/C2JM30341H



**9 AUTHORS**, INCLUDING:

Antonio De Luca
Università della Calabria
**77** PUBLICATIONS **1,246** CITATIONS
SEE PROFILE

Mélanie Ferrié
Centre de Recherche Paul Pascal
**7** PUBLICATIONS **50** CITATIONS
SEE PROFILE

Melissa Infusino
Universidad San Francisco de Quito (USFQ)
**19** PUBLICATIONS **56** CITATIONS
SEE PROFILE

Giuseppe Strangi
Case Western Reserve University
**108** PUBLICATIONS **866** CITATIONS
SEE PROFILE

Journal of Materials Chemistry

Cite this: J. Mater. Chem., 2012, 22, 8846

www.rsc.org/materials

PAPER

# Gain functionalized core–shell nanoparticles: the way to selectively compensate absorptive losses

Antonio De Luca,*[a] Mélanie Ferrie,[b] Serge Ravaine,[b] Massimo La Deda,[c] Melissa Infusino,[a] Alireza R. Rashed,[a] Alessandro Veltri,[b] Ashod Aradian,[b] Nicola Scaramuzza[a] and Giuseppe Strangi[a]

*Received 17th January 2012, Accepted 27th February 2012*
**DOI: 10.1039/c2jm30341h**



We experimentally demonstrate that gain materials properly encapsulated into the shell surrounding metal nanoparticles (NPs) are responsible for the modification of the overall plasmon response of engineered nanostructures. A comparison between designed systems based on functionalized core–shell NPs having different encapsulated dye molecules is presented. Experimental observations of Rayleigh scattering enhancement, accompanied by an increase of transmission as a function of gain, reveal striking optical loss compensation effects. Fluorescence lifetime measurements demonstrate a quenching of dye photoluminescence in functionalized core–shell NP samples with respect to pure dye solutions, confirming the strong resonant coupling occurring between the gain medium and gold NPs. Experimental evidence of a selective modification of the gain functionalized core–shell Au NP extinction curve is found, in good agreement with the results of a simplified theoretical model. The model verifies the causality principle through Kramers–Kronig dispersion relations for the investigated gain functionalized plasmonic nanostructure.

## 1 Introduction

Research on plasmonic systems consisting of noble metal nanoparticle assemblies represents a central topic in the field of optoelectronics, such as light-emitting diodes, waveguides, and nanolasers, primarily owing to the unique property known as localized surface plasmon resonance (LSPR) exhibited by metallic nanostructures.[1–8] In studies on spontaneous emissions, both fluorescence enhancement and quenching have been observed for fluorophores in the vicinity of metallic nanostructures.[7,8] The enhancement factor is largely dependent on the distance between fluorophores and metal, because the radiative and nonradiative transitions of fluorophores vary significantly with their spatial separation.[7] As a result, it is usual that the maximum enhancement is not around the metallic surface but in a region a few nanometers away.[8] Recently, resonance energy transfer between dye molecules and metal nanoparticles has gained interest in finding potential application in nano-optics, biophotonics and solar cells.[9–11] In a recent experimental study, Strouse and co-workers found that the rate of energy transfer from a dye to a gold nanoparticle inside DNA has a $1/d^4$ distance dependence, thus it is considered as a surface energy transfer (SET) process.[12,13] Several theoretical and experimental studies have been published on energy transfer from a dye to a metal surface.[12–21] Chance *et al.*[16] described the process of the rate of energy transfer from a dye molecule to a metallic surface as SET and they have predicted that the separation has a $d^{-4}$ dependence. According to their model, the exact form of the dipole–surface energy transfer rate is given by: $k_{SET} = 1/\tau_D(d_0/d)$,[4] where $\tau_D$ is the lifetime of the donor in the absence of the acceptor, $d$ is the distance between the donor and acceptor, and $d_0$ is known as the Förster distance, the distance at which the transfer rate $k(r)$ is equal to the decay rate of the donor in the absence of the acceptor, in a Förster like resonant energy transfer mechanism. According to Förster theory,[22] the rate of energy transfer through the dipole–dipole interactions between an excited donor (D) molecule and an acceptor (A) is given by $k_T = 1/\tau_D(R_0/r)$.[6] However, the Förster resonance energy transfer (FRET) technique is restricted to an upper limit of separation of only 80 Å, the energy transfer becoming too weak beyond this distance.[23] If you chemically encapsulate the donor inside a shell surrounding the metal nanoparticles, you can achieve the result of having the donor at a fixed distance (or better as a homogeneous distribution inside the shell). By considering the theory proposed by Bhowmick *et al.*,[19] you can continue to find that Coulombic energy transfer to the surface plasmonic modes indeed has the Förster $d^{-6}$ distance dependence at large separation between the dye and the nanoparticle, even if, for distances comparable to the size of the nanoparticle, they found the distance dependence of the rate varies as $d^{-\sigma}$, with $\sigma$ between 3 and 4 (as for a SET process).

[a]*Department of Physics, CNR-IPCF UOS di Cosenza, Licryl Laboratory-University of Calabria, 87036-Rende, Italy. E-mail: antonio.deluca@fis.unical.it; giuseppe.strangi@fis.unical.it*
[b]*CRPP - Centre de Recherche Paul Pascal, CNRS, University Faculty Bordeaux 1, Bordeaux, France*
[c]*Department of Pharmaceutical Sciences, and CEMIF.CAL, 87036 Rende, CS, Italy*

In particular, based on the arguments proposed in ref. 19 and 24, we can consider a donor dye molecule emitting in the visible range (520–630 nm, with a transition that corresponds to 1.97 eV $< E_2 - E_1 <$ 2.39 eV). The acceptor is a nanoparticle with plasma frequency $\omega_p \sim 6.7 \times 10^{14}$ s$^{-1}$ ($\lambda \sim 450$ nm, as evidenced by experimental studies and theoretical predictions). The plasmon frequencies $\omega_l$ for the pertinent localized surface modes depend on the size of the nanoparticle and they are related to plasma frequency by:

$$\omega_l = \omega_p \sqrt{\frac{l+1}{2l+1}} \quad (1)$$

$l$ being the orbital quantum number. This clearly implies that frequencies of the surface modes are lower than $\omega_p$ ($\omega_l/\omega_p \sim 0.8$ for 12 nm NP core size,[24]), and that the $l = 1$ surface plasmon modes are centered around 550 nm, red-shifted (about 20 nm) with respect to the measured maximum of the plasmon band. These considerations show that, for gold nanoparticles in the range of 5–10 nm radius, the "dipolar" mode ($l = 1$) is the predominant accepting mode for energy transfer with a dye emitting in the visible range from 500–600 nm. Other surface plasmon modes ($l = 2$, centered around 580 nm) might be involved in the resonant energy transfer process in case the emission band of the encapsulated fluorophores overlaps these modes. Therefore, the dye–Au NP resonance band for effective energy transfer which can lead to a high coupling between the two species is separately always red-shifted with respect to the plasmon band maximum (relative to the $l = 0$, bulk mode).

Here we report an experimental study aim at showing that encapsulating gain media into the shell surrounding a metal nanoparticle can induce a Förster like resonant energy transfer process from the excitonic medium to the plasmon modes of the metal NPs. This enables a huge enhancement of the local excitation field as well as a modification of the radiative and nonradiative decay rates of the fluorophores, inducing a remarkable quenching of fluorescence. Excitation energy transfer occurs uniquely *via* a resonant nonradiative process involving simultaneous de-excitation of dye molecules and excitation of plasmon NPs resulting in a quasistatic electric field energy of SPs. In particular, the investigations were performed on core–shell gold nanospheres functionalized by encapsulating proper gain units into silica shells surrounding the NPs. Induced optical transparency accompanied by a considerable enhancement of the Rayleigh scattering intensity as a function of the gain are presented. Fluorescence lifetime measurements have demonstrated remarkably different quenching behaviors for the investigated systems, as evidenced by the partial or absolute (a few thousand counts) absence of an emission signal. A broadband spectroscopic study of the designed nanostructures provided absorbance curves for both systems, revealing selective wavelength behavior as function of the gain. Kramers–Kronig relations for the effective permittivity of the system is provided by two similar areas marked in the last figure. The obtained results demonstrate an important selective mitigation effect in metal NPs engineered as building blocks to create low loss optical metamaterials. A simple model is proposed to evidence that in the case of a single gold core–shell NP, by adding gain into the silica shell it is possible to predict the modification of the calculated absorbance curve that follows the same behavior of the experimental data.

## 2 Results and discussion

Experiments have been performed through a systematic approach either to evaluate known effects which arise during resonant energy transfers or by measuring key physical quantities as function of excitation energy. Rayleigh scattering and transmission of a probe beam propagating through the excited volume were measured to verify the gain induced changes of NP absorption. The optical excitation of fluorescent guest molecules is followed either by radiative or nonradiative decays. In case of dye–NP coupling the probability of nonradiative decay can assume a very high rate ($R_{nonrad}$), so that it may become the main decay channel of the excited dye molecules. Then, the radiative decay rate ($R_{rad}$) can be reduced to a small fraction of the total decay rate, producing a considerable effect of fluorescence quenching due to:[18]

$$R_{fluo}(r) = R_{rad}(r) + R_{nonrad}(r) \quad (2)$$

Gain functionalized ($G_f$) metal nanoparticles consist of a gold core (diameter $d \sim 12$ nm) coated with a silica shell (12 nm thick) containing organic dye molecules.[14] Two photostable organic dyes (Coumarin C500 and DCM by Exciton, chemical formulae in the insets of Fig. 1(a) and (b), respectively) were chemically encapsulated into the shell, creating two functionalized systems: Au@$SiO_2$/C500 ($G_f$-C500) and Au@$SiO_2$/DCM ($G_f$-DCM). The two systems were optically excited by laser pulses at 355 nm, a wavelength far from the maximum of the NP extinction band, showing a completely different gain curve overlapping with the plasmon band of gold NPs (black lines in Fig. 1). As we can see, the emission curves of the two dyes are considerably different, presenting a maximum at 500 nm (C500) and 630 nm (DCM), a spectral position blue shifted with respect to the plasmon band for C500, whereas it is red shifted for DCM. We studied how the different overlapping spectra affect the coupling strength and the energy transfer processes between the gain medium and metal NPs. As observed by Dulkeith *et al.*,[20] if a donor fluorescent molecule is maintained in the vicinity of a metal nanoparticle, a drastic quenching of fluorescence is expected. This effect was predicted by Gersten and Nitzan by considering a remarkable enhancement of nonradiative resonant energy transfer between donor fluorophore and plasmonic acceptor.[18] In order to perform a comparative analysis of gain induced optical loss modifications, pump–probe experiments have been carried out on the two systems, along with time-resolved fluorescence spectroscopy. According to the Beer–Lambert law, by measuring simultaneously Rayleigh scattering and transmission, either in the absence or in the presence of gain, we should be able to understand if the absorptive power of the material is affected by excitation energy transfer. Thus, modifications of the Rayleigh scattering and transmitted intensity of a constant probe beam ($\lambda_p = 532$ nm for $G_f$-C500 and $\lambda_p = 600$ nm for $G_f$-DCM) have been monitored as a function of the pump energy for both systems (excitation @ 355 nm). As first proposed by Lawandy,[25] the localized surface plasmon (LSP) resonance in metallic nanospheres is predicted to exhibit a singularity when the surrounding dielectric medium has a critical value of optical gain. This can be evidenced by an increase of the Rayleigh scattering signal because of the enhancement of the local field surrounding

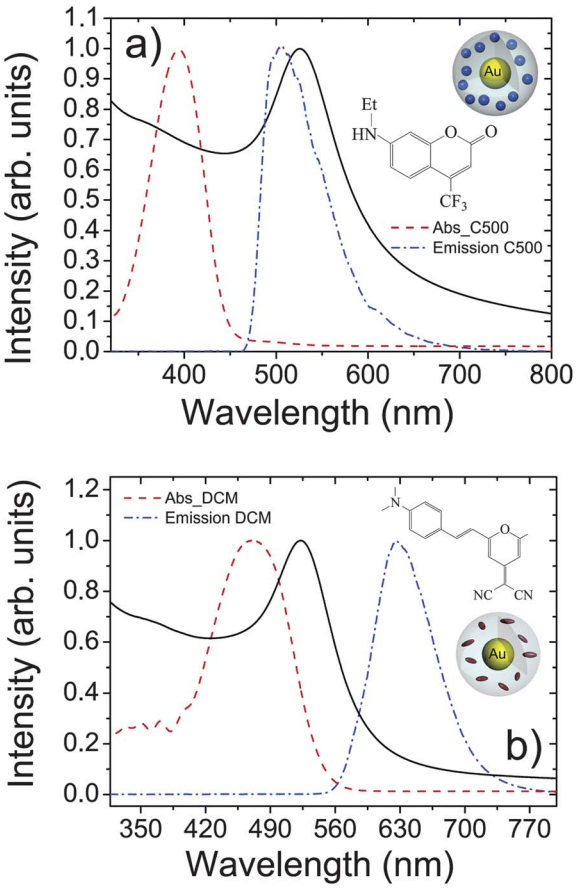


**Fig. 1** a) Absorption (red dash) and emission (blue dash dot) spectra of C500 dye dissolved in ethanol and plasmon band (black line) of $G_f$-C500 gold nanoparticles. b) Absorption (red dash) and emission (blue dash dot) spectra of DCM dye dissolved in ethanol and plasmon band (black line) of $G_f$-DCM gold nanoparticles.

the nanoparticle. Hence, a pump–probe Rayleigh scattering experiment enables us to observe the enhancement of the SP resonance due to the gain material chemically encapsulated in the silica shell surrounding the gold core. Pump–probe Rayleigh scattering experiments were performed by launching co-linearly a probe beam in a small portion of the volume excited by a wider pump spot at $\lambda = 355$ nm (Fig. 2). The scattered probe light, acquired by means of the optical fiber of a high-resolution spectrometer (HORIBA Jobin-Yvon MicroHR Symphony), was observed in the spectrum as a relatively narrow line centered at 532 nm or 600 nm. Fig. 3(a) shows the difference between the maximum of the scattered beam and the corresponding value in the residual fluorescence emission spectrum for system $G_f$-C500 (S in Fig. 2), plotted as a function of the pump energy. The super-linear increase of the scattered signal (RS in Fig. 2) above a certain threshold value of gain is a demonstration of the enhancement of the quality factor of SP resonance mediated by resonant energy transfer processes between active elements and gold cores within the composite NPs. The presence of a threshold gain value above which systems show non-linear behavior was already discussed by Lawandy,[25] arguing that a singularity in the NP local field is expected as the transferred energy compensates the absorptive losses by exciting NP surface plasmon modes.

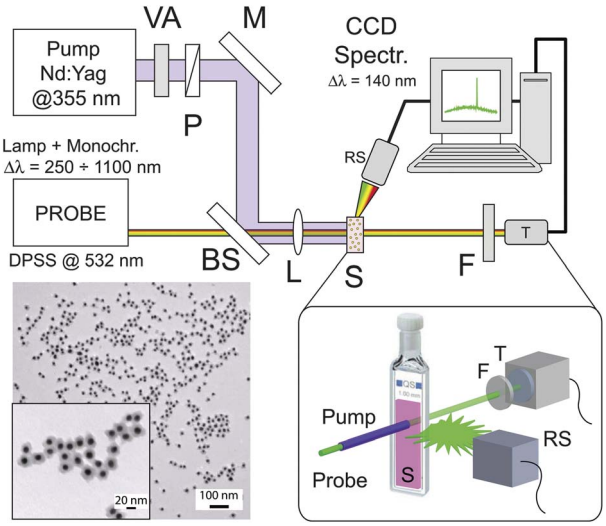


**Fig. 2** Pump–probe experimental set-up. VA: variable attenuator, P: polarizer, M: mirror, BS: beam splitter, L: lens, S: sample, F: filter, RS: Rayleigh scattering detector, T: transmission detector, DPSS: diode-pumped solid state laser CW. TEM images of the obtained core–shell NPs with silica shell are shown at different scales for both $G_f$-C500 (inset at 20 nm scale) and $G_f$-DCM (100 nm scale) samples. The size of the metal core and the thickness of the silica shell were both measured by statistical analysis of TEM pictures.

However, the key experiment of this work was performed by simultaneously measuring the transmission at the far field of the probe waves after passing the excited volume with a different level of gain, selected by varying the pump rate.

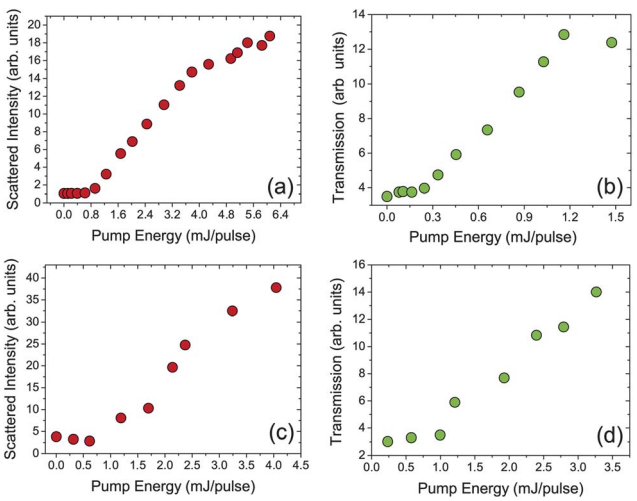


**Fig. 3** Comparison of scattering and transmission enhancement signals between the $G_f$-C500 (a and b) and $G_f$-DCM (c and d) systems. Enhancement of SP is evidenced by an increase of the normalized Rayleigh scattering signal of a probe beam ($\lambda = 532$ nm for $G_f$-C500 (a) and $\lambda = 600$ nm for $G_f$-DCM (c)) as a function of pump energy ($\lambda = 355$ nm). Normalized transmission increase of a probe beam as a function of pump energy for (b) $G_f$-C500 at 532 nm and for $G_f$-DCM at 600 nm (d). Comparable threshold values for scattering signals have been observed, whereas a lower transmission threshold for $G_f$-C500 is observed with respect $G_f$-DCM.

Fig. 3(b) shows the increase of transmission peaks of the probe signal at 532 nm as a function of the excitation energy (T in Fig. 2), evidencing a clear gain-induced transparency of the whole system. A pin-hole and a notch filter (F in Fig. 2) provide the best conditions to avoid stray light and any other undesired contribution to the transmitted light. A comparative set of measurements (both scattering and transmission) have been performed on system $G_f$-DCM (S in Fig. 2), revealing similar threshold values with respect to the first one. Fig. 3(c) and (d) show Rayleigh scattering intensity and transmission at the probe wavelength of 600 nm, as a function of the pump rate in the $G_f$-DCM system. By considering a few percent of the occupied volume ratio (~10%) and the volume of a single dye molecule, we estimated $10^3$–$10^4$ molecules encapsulated per single nanoparticle in both cases, an amount sufficient to permit an effective non-radiative energy transfer to gold NPs and promote excitation of the surface plasmon modes, by providing an estimated local gain of about $10^4$–$10^5$ $cm^{-1}$.[25] To corroborate evidence of mitigation of absorptive losses in $G_f$ core–shell NPs, time-resolved fluorescence spectroscopy has been carried out on both systems, proving dye–NP coupling and energy transfer processes. Fluorescence lifetime measurements have demonstrated quenching behavior, consistent with a small separation distance between the dye and the surface of the nanoparticle, because of their strong resonant coupling. Fig. 4 reports time-correlated single-photon counting (TCSPC) data acquired at 498 nm for $G_f$-C500 and at 626 nm for $G_f$-DCM with respect to the pure C500 and DCM dye solutions, when irradiated with a 265 nm or 379 nm NanoLed pulsed laser-diode, respectively. The time-resolved fluorescence intensity decay of the ethanol solution of pure C500 molecules has been fitted as a single exponential function in Fig. 4(a) (red dots and green line fit), giving a time constant of $\tau_{fluo-C500} = 5.42 \pm 0.01$ ns ($\chi^2 = 0.997$). The same measurement made on the DCM solution gave a time constant of $\tau_{fluo-DCM} = 1.682 \pm 0.005$ ns ($\chi^2 = 0.995$). From the TCSPC data of the $G_f$ systems (black dots and cyan line fits), two components can be identified in the decay dynamics, but only for the $G_f$-C500 system. A fast decay is accompanied by a long-living emission where the decay kinetics resembles the fluorescence decay for pure gain dye molecules (see Table 1 for details). The first decay time is attributed to the fraction of dye molecules encapsulated in the silica shell that experience the resonant energy transfer process; the long-living emission is related to that fraction present in the shell that are not coupled to plasmonic nanoparticles.

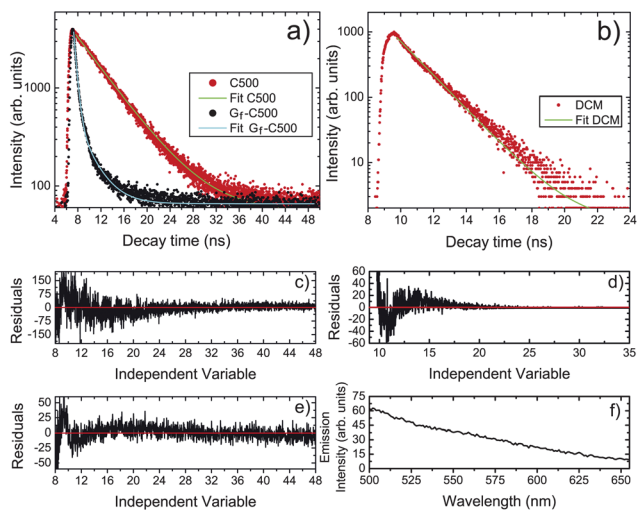


**Fig. 4** Time-resolved fluorescence intensity decays: $G_f$-C500 (a) and $G_f$-DCM (b) systems are compared to pure dye solutions of C500 and DCM, respectively. The long-living emission of pure C500 is characterized by a time constant $\tau_{fluo-C500} = 5.42$ (red dots and green fit). Two components are identified in the decay dynamics of the $G_f$-C500 system: $\tau_{1-C500} \sim 2.78$ ns and $\tau_{2-C500} \sim 0.5$ ns (black dots and cyan fit). (c) and (e) represent the residuals obtained for the C500 and $G_f$-C500 decay fits, respectively. (b) contains only the decay of DCM dye, because of an absence of an emission signal in the $G_f$-DCM system. (d) and (f) contain residuals for the DCM decay fit and the very low emission acquired for the $G_f$-DCM system (excitation 379 nm, cut-off 450 nm), respectively.

The intensity emission decays for this system have been fitted as two bi-exponentials. The short-living time constant ($\tau_2 = 0.508$ ns) is one order of magnitude lower than that of the pure dye solution (see Table 1), whereas the long-living decay time ($\tau_1 = 2.78$ ns) is in the same range. The identification of two exponential decays indicates incomplete dye–NP coupling for the $G_f$-C500 system, though the presence of a reduced decay time is attributed to a significant decrease of the radiative rate due to the fraction of dye molecules, encapsulated into the silica shell, that experiences the resonant energy transfer process. This elucidates the nonradiative energy transfer rate as a consequence of strong coupling for this $G_f$ system, representing a clear demonstration that gain is brought to plasmonic NPs. Residuals for the pure dye solution and $G_f$-C500 system are reported in Fig. 4(c) and (e). On the contrary, as evidenced by the absence of data for the $G_f$-DCM system in Fig. 4(b), we had no chance to observe any significant emission (see Fig. 4(f)) at 626 nm for this sample. This implies that we were not able to perform fluorescence lifetime measurements at all, indicating that DCM dye present in the shell experienced complete fluorescence quenching. Fig. 4(d) shows residuals for the DCM dye solution, whereas Fig. 4(f) represents the signal acquired as fluorescence emission (excitation 379 nm, cut-off 450 nm to avoid multiple wavelength generation) of the $G_f$-DCM system (a few thousand counts, that can be considered zero). However, the key experiment of this work was performed by measuring the transmitted intensity at the far field of the broadband probe light-waves after passing the excited volume with a fixed level of gain, selected by fixing the pump rate. Then, the transmitted intensity was also acquired at different wavelengths (by using a xenon based lamp with a monochromator by LOT-Oriel Group) in the presence and absence of the pump beam, to emphasize the changes of absorptive power induced by energy transfer during dye excitation. In Fig. 5(a) we plotted the difference ($\Delta T = T_p - T_{wp}$, orange dots) between the transmitted signal in the presence ($T_p$) of the pump and that in the absence ($T_{wp}$) of the pump beam, as a function of wavelength. The same figure shows the plasmon band (black line) and C500 dye emission (green line) in order to identify the overlapping region. Fig. 5(b) represents the retrieved data from Fig. 5(a) utilized to reconstruct the extinction band for the $G_f$-C500 system in the absence (black dots) and presence (red dots) of gain (pump beam on) calculated as $Abs = \log_{10}(I_T/I_i)$, where $I_T$ is the transmitted intensity and $I_i$ is the incident intensity on the sample. It is shown that the difference $\Delta T$ assumes negative values in the wavelength range 460–530 nm, whereas after 530 nm $\Delta T$ starts to became

**Table 1** Time resolved fluorescence decay for $G_f$-C500 and $G_f$-DCM systems with respect to the pure dye solutions

| | Excitation/nm | Emission/nm | $\chi^2$ | $\tau_1$(ns) | $\tau_2$(ns) |
|---|---|---|---|---|---|
| C500-EtOH | 265 | 498 | 0.997 | 5.42 ± 0.01 | |
| $G_f$C500 | 265 | 498 | 0.998 | 2.78 ± 0.05 | 0.508 ± 0.003 |
| DCM-EtOH | 379 | 626 | 0.995 | 1.682 ± 0.005 | |
| $G_f$-DCM | 379 | 626 | — | no emission | no emission |

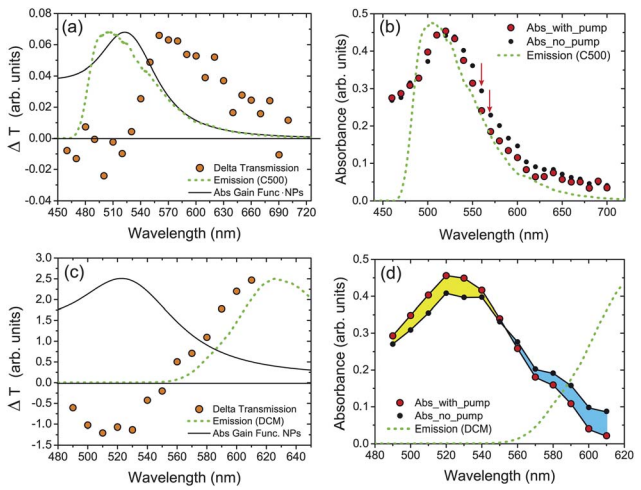


**Fig. 5** Broadband delta of transmission measurements of the two $G_f$ systems ($G_f$-C500 (a) and $G_f$-DCM (c)). $\Delta T = T_p - T_{wp}$, where $T_p = T$ with pump, and $T_{wp} = T$ without pump. (b) and (d) represent the retrieved data from (a) and (c) utilized to reconstruct the extinction band for the two systems in the absence (black dots) and presence (red dots) of gain (pump beam on) calculated as Abs = $\log_{10}(I_T/I_i)$.

positive ($T_p > T_{wp}$). This is even better evidenced by the extinction bands reported in Fig. 5(b): the absorption of the whole excited system decreases with respect to the non-excited one, revealing the occurrence of a nonradiative energy transfer process. The same measurements were performed on the $G_f$-DCM system, that experienced an extinction band more blue-shifted and with a smaller overlapping area with respect to the dye emission curve (green curve in Fig. 5(c)). In this case, $\Delta T$ starts to assume positive values exactly in correspondence with the rise of the DCM emission curve, where spectral overlapping starts to became non-zero, showing a marked distinction between negative and positive values (orange dots). The measured curves related to the absorption bands for the $G_f$-DCM system in the presence (red dots) and in the absence of the pump beam (black dots in Fig. 5(d)) clearly show how below 550 nm the whole system experienced higher values for the extinction curve in the presence of gain. This is compensated by the modification of the curve above 550 nm, where absorption is reduced by supplying gain to the system as evidenced by lower values for extinction curve with respect to those obtained in the absence of an exciting optical field. These two results obtained in gain functionalized systems, with the assistance of two different gain media, experimentally emphasize that modifications of the imaginary part of the permittivity $\varepsilon_{im}(\omega)$, that is directly related to the absorption, clearly depend on gain–surface plasmon mode spectral overlap. A reduction of absorption in a band (*i.e.* between 550–610 nm, cyan area in Fig. 5(d)) corresponds to an increase of the same quantity in a complementary wavelength band (490–550 nm, yellow area in Fig. 5(d)), in good agreement with the results of a theoretical model accounting for the coupling between gain and plasmonic nanoparticles upon verifying the causal nature of the response of materials *via* Kramers–Kronig (KK) dispersion relations.

## 3 Theoretical model

In order to obtain the absorbance behavior of a core–shell system in the presence of gain we used a very simple model that takes into account the principle of causality through Kramers–Kronig relations. The quasi-static expression for the polarizability of a core–shell particle of internal radius $r_1$ and external radius $r_2$, having $\varepsilon_1$, $\varepsilon_2$ and $\varepsilon_3$ as the complex permittivity of the core, the shell and the external medium, respectively,[26] can be written as:

$$\alpha = 4\pi r_2^3 \frac{(\varepsilon_2 - \varepsilon_3)(\varepsilon_1 + 2\varepsilon_2) + \rho^3(\varepsilon_1 - \varepsilon_2)(\varepsilon_3 + 2\varepsilon_2)}{(\varepsilon_2 + 2\varepsilon_3)(\varepsilon_1 + 2\varepsilon_2) + 2\rho^3(\varepsilon_2 - \varepsilon_3)(\varepsilon_1 - \varepsilon_2)} \quad (3)$$

where $\rho = \frac{r_1}{r_2}$. Here we used a spline interpolation of the Johnson and Christy dataset for gold[27] to describe $\varepsilon_1(\omega)$ and a single symmetric gain line susceptibility description for $\varepsilon_2(\omega)$:

$$\varepsilon_2(\omega) = \varepsilon_H - \frac{\varepsilon_2''(\omega_0)\Delta}{2(\omega - \omega_0) + i\Delta} \quad (4)$$

where $\varepsilon_H$ is the permittivity of the host in which the gain is dissolved, $\varepsilon_2''(\omega_0)$ corresponds to the maximum value for the imaginary part of the gain functionalized host permittivity, $\Delta$ is the bandwidth and $\omega_0$ the center of the line for the used dye. For the sake of simplicity we used a dye having an emission band centered in the plasmonic resonance, with a bandwidth comparable with the one of the plasmon without gain. For $\varepsilon_H$ and for $\varepsilon_3$ we used the values of silica and ethanol ($\varepsilon_H = 2.1316$, $\varepsilon_3 = 1.8496$). Using eqn (3), it is possible to calculate the absorption cross section of our nanoparticle as:

$$\sigma = \frac{2\pi\sqrt{\varepsilon_3}\alpha''}{\lambda}, \quad (5)$$

from which we can finally calculate the absorbance of the system:

$$A = \frac{\sigma n L}{\ln(10)}, \quad (6)$$

where $n$ is the density of nanoparticles ($n = \rho/W_c$, where $W_c$ is the weight of the gold core, given by $W_c = \frac{4\pi}{3} r_1^3 \rho_0$, $\rho = 0.38$ g L$^{-1}$ and $\rho_0 = 0.193$ g L$^{-1}$) and $L = 1$ mm, the thickness of the sample. By considering values of $r_1 = 0.6$ nm and $r_2 = 0.4$ nm, the simplified model predicts the absorbance behavior for the system in the absence of gain ($\varepsilon_2''(\omega_0) = 0$) that is reported in Fig. 6 (black



 

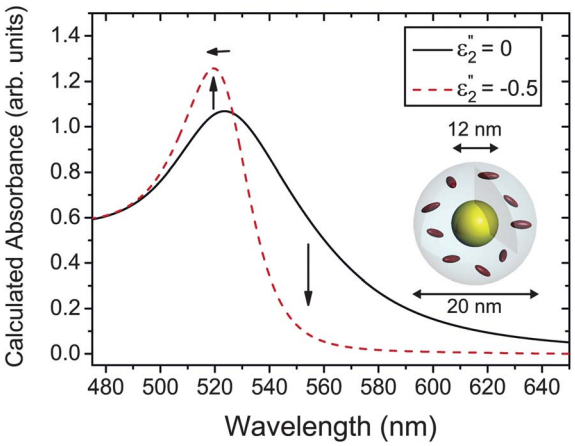


**Fig. 6** Calculated absorbance of a gold core/silica shell (12 nm/4 nm) with dye encapsulated into the shell. $\varepsilon_2''(\omega_0) = 0$ means zero gain, whereas $\varepsilon_2''(\omega_0) = -0.5$ means a certain gain considered into the silica shell.

solid line). By adding a certain amount of gain into the shell ($\varepsilon_2''(\omega_0) = -0.5$), the model predicts the modification of the absorbance curve (red dash line in Fig. 6) in a way that follows the same behavior of the experimental data reported in Fig. 5d, including the slight maximum blue shift. The calculated absorbance reported in Fig. 6 is relative to a gain encapsulated silica shell thickness of 4 nm.[28] This choice is due to the fact that only fluorophores in close proximity are strongly coupled with the plasmon gold core, then promoting a remarkable resonant energy transfer process. However, a more detailed model that consider the distribution of dye molecules in the shell, including a more precise coupling effect between NPs and organic molecules, will be presented elsewhere.

## 4 Conclusions

In conclusion, two gain functionalized systems have been compared, based on the inclusion of different dye molecules in the shell surrounding the nanoparticle gold core. Although the Rayleigh scattering and transmission enhancement is comparable for the two systems, the different spectral position of the emission curves of the gain molecules reveals a different band overlapping with the gold nanoparticles extinction band. Also time-resolved fluorescence decay curves, performed on both systems ($G_f$-C500 and $G_f$-DCM), emphasize a remarkable coupling difference as evidenced by the complete fluorescence quenching only for the DCM present in the shell. Striking evidence of selective compensation of absorptive optical losses is provided by measuring the difference between the transmitted signal in the presence ($T_p$) of the pump with respect to that in the absence ($T_{wp}$) of the pump beam. The measurements carried out in the spectral range 460–700 nm allow us to reconstruct Abs curves for the two systems in the presence and absence of gain (pump energy). Optical transmission turns out to be enhanced selectively within the band where resonant energy transfer by the gain medium to plasmonic nanoparticles occurs. According to Kramers–Kronig relations these permittivity modifications induced in a limited spectral region are expected to modify also the response in close spectral bands. Differential absorption curves, as well as the retrieved absorbance, show exactly this behavior. Taking into account the principle of causality through Kramers–Kronig relations, the presented model reveals the possibility to predict this behavior in a simple way, by considering a single gold core/silica shell nanoparticle with gain encapsulated into the shell (negative value for $\varepsilon_2''(\omega_0)$), resulting in good agreement with the experimental data.

## 5 Methods

### 5.1 Chemicals

12 ± 2 nm gold nanoparticles were synthesized through the reduction of hydrogen tetrachloroaurate (III) ($HAuCl_4$) in the presence of sodium citrate ($Na_3C_6H_5O_7 \cdot 2H_2O$) according to the procedure published by Grabar *et al.*[29] The gold nanoparticles were coated with a 12 ± 2 nm fluorescent silica shell according to the procedure published by Graf *et al.*[30] Briefly, 0.15 g of polyvinylpolypyrrolidone (PVP K15, Mw ~ 10000) in 5 ml of water was added to 100 ml of the aqueous solution of gold nanoparticles ($2.71 \times 10^{15}$ particles $l^{-1}$). The reaction occurred at room temperature in the dark under continuous stirring for 12 h. PVP-capped gold nanoparticles were collected by centrifugation (16000 rpm for 1 h) and redispersed in 10 mL of ethanol. 100 mL of an ethanolic solution of tetraethylorthosilicate (TEOS, 0.2 mM)) and C500 ($7.7 \times 10^{-3}$ mM) or DCM ($10^{-3}$ mM) were then added to this solution. The reactive medium was stirred in the dark for two hours before the addition of 10 ml of ammonia (25% in water). The reaction occurred at room temperature in the dark under continuous stirring for over 24 h. The core–shell particles were collected and washed through three cycles of centrifugation (16000 rpm for 1 h at room temperature) and redispersed in absolute ethanol. At the end of the washing cycles, the fluorescence of the supernatant was measured. No significant signal was detected, indicating that dye leaching to solution did not occur.

### 5.2 Characterization and measurements

Extinction bands were measured by means of a spectrophotometer (Cary500 by Varian), whereas the fluorescence emission was acquired by a high sensitivity spectrometer (SPM-002-ET 200–1090 nm, Hamamatsu S9840 Back-Thinned CCD by Photon Control). Furthermore, Förster nonradiative energy transfer processes necessary to mitigate the high metal losses can be observed through indirect experiments. All of them are based on a pump–probe set-up. The sample is optically pumped with 4 ns pulses of a third harmonic Nd:YAG laser (Brio by Quantel), $\lambda =$ 355 nm. A probe beam (Diode-Pumped Solid-State Laser @ 532 nm by Laser Quantum for the $G_f$-C500 system and xenon based lamp with a monochromator by LOT-Oriel Group, $\lambda =$ 600 nm for the $G_f$-DCM system), with a fixed power, was focused within the pumped region of the sample. The probe wavelength was chosen in the proximity of the overlapping region between dye fluorescence and plasmon band maxima, where localized surface plasmon modes are expected. The probe light emitted, scattered or transmitted by Au NPs ($\lambda = 532$ nm or $\lambda = 600$ nm) was collected by an optical fiber together with the emission of the dye, in a position depending on the particular experiment. The fiber was positioned at an angle of 70° relative to the beam

propagation direction for the scattering (90° for the fluorescence) experiment, within several millimeters of the cuvette. The transmission signal was acquired far from the sample, on the same pump beam direction and with a high neutral filter in front of the fiber head, in order to prevent any possible signal different from the probe one (high stable power). The fluorescence lifetime of the two systems was acquired, with respect to that of the pure dye solution, by means of a time-resolved spectrofluorometer (pump @ 265 nm/379 nm of NanoLed pulsed laser-diodes, emission at 498 nm/626 nm respectively, HORIBA Jobin-Yvon Fluorolog-3 FL3-211), using the time-correlated single-photon counting (TCSPC) option. Excitation sources were mounted directly on the sample chamber at 90° to a single-grating emission monochromator (2.1 nm $mm^{-1}$ dispersion; 1200 grooves $mm^{-1}$) and collected with a TBX-04-D single-photon-counting detector. The photons collected at the detector were correlated by a time-to-amplitude converter (TAC) to the excitation pulse. Signals were collected using an IBH Data Station Hub photon counting module, and data analysis was performed using the commercially available DAS6 software (HORIBA Jobin Yvon IBH). Quality of fit was assessed by minimizing the reduced $\chi^2$ function and visual inspection of the weighted residuals.

## Acknowledgements

The authors thank C. Versace for the fruitful scientific discussions. The research leading to these results has received funding from the European Union's Seventh Framework Programme (FP7/2008) Metachem Project under Grant Agreement No. 228762.

## References

1 K. Okamoto, I. Niki, A. Shvartser, Y. Narukawa, T. Mukai and A. Scherer, *Nat. Mater.*, 2004, **3**, 601–605.
2 F. Tam, G. P. Goodrich, B. R. Johnson and N. J. Halas, *Nano Lett.*, 2007, **7**, 496–501.
3 W. L. Barnes, A. Dereux and T. W. Ebbesen, *Nature*, 2003, **424**, 824–830.
4 V. J. Sorger, R. F. Oulton, J. Yao, G. Bartal and X. Zhang, *Nano Lett.*, 2009, **9**, 3489–3493.
5 M. A. Noginov, G. Zhu, A. M. Belgrave, R. Bakker, V. M. Shalaev, E. E. Narimanov, S. Stout, E. Herz, T. Suteewong and U. Wiesner, *Nature*, 2009, **460**, 1110–1113.
6 R. F. Oulton, V. J. Sorger, T. Zentgraf, R. Ma, C. Gladden, L. Dai, G. Bartal and X. Zhang, *Nature*, 2009, **461**, 629–632.
7 P. Bharadwaj and L. Novotny, *Opt. Express*, 2007, **15**, 14266–14274.
8 O. G. Tovmachenko, C. Graf, D. J. van den Heuvel, A. van Blaaderen and H. C. Gerritsen, *Adv. Mater.*, 2006, **18**, 91–95.
9 Y. Chiu, S. Chen, J. Chen, K. Chen, H. Chen and H. Sung, *ACS Nano*, 2010, **4**, 7467–7474.
10 J. I. Basham, G. K. Mor and C. A. Grimes, *ACS Nano*, 2010, **4**, 1253–1258.
11 G. K. Mor, J. Basham, M. Paulose, S. Kim, O. K. Varghese, A. V. S. Yoriya and C. A. Grimes, *Nano Lett.*, 2010, **10**, 2387–2394.
12 C. S. Yun, A. Javier, T. Jennings, M. Fisher, S. Hira, S. Peterson, B. Hopkins, N. O. Reich and G. F. Strouse, *J. Am. Chem. Soc.*, 2005, **127**, 3115–3119.
13 T. L. Jennings, M. P. Singh and G. F. Strouse, *J. Am. Chem. Soc.*, 2006, **128**, 5462–5467.
14 G. Strangi, A. De Luca, S. Ravaine, M. Ferrie and R. Bartolino, *Appl. Phys. Lett.*, 2011, **98**, 251912.
15 A. De Luca, M. P. Grzelczak, I. Pastoriza-Santos, L. M. Liz-Marzán, M. L. Deda, M. Striccoli and G. Strangi, *ACS Nano*, 2011, **5**, 5823–5829.
16 R. Chance, A. Prock and R. Silbey, *Adv. Chem. Phys.*, 1978, **60**, 1.
17 B. N. Persson and N. D. Lang, *Phys. Rev. B*, 1982, **26**, 5409.
18 J. Gersten and A. Nitzan, *J. Chem. Phys.*, 1981, **75**, 1139–1152.
19 S. Bhowmick, S. Saini, V. B. Shenoy and B. Bagchi, *J. Chem. Phys.*, 2006, **125**, 181102.
20 E. Dulkeith, A. C. Morteani, T. Niedereichholz, T. A. Klar, J. Feldmann, S. A. Levi, F. C. J. M. van Veggel, D. N. Reinhoudt, M. Moller and D. I. Gittins, *Phys. Rev. Lett.*, 2002, **89**, 203002.
21 A. P. Alivisatos, D. H. Waldeek and C. B. Harris, *J. Chem. Phys.*, 1985, **82**, 541.
22 T. Förster, *Ann. Phys.*, 1948, **2**, 55–75.
23 J. R. Lakowicz, *Principles of Fluorescence Spectroscopy*, Springer, New York, 2006, 3rd edn, p. 444.
24 J. M. Pitarke, V. M. Silkin, E. V. Chulkov and P. M. Echenique, *Rep. Prog. Phys.*, 2007, **70**, 1–87.
25 N. M. Lawandy, *Appl. Phys. Lett.*, 2004, **85**, 5040–5042.
26 D. R. H. Craig and F. Bohren, *Absorption and Scattering of Light by Small Particles*, WILEY-VCH Verlag GmbH & Co. KGaA, 1998.
27 P. Johnson and R. Christy, *Phys. Rev. B: Solid State*, 1972, **6**, 4370–4379.
28 A. Veltri and A. Aradian, *Phys. Rev. B*, 2012, DOI: 10.1103/PhysRevB.00.003400.
29 K. C. Grabar, R. G. Freeman, M. B. Hommer and M. J. Natan, *Anal. Chem.*, 1995, **67**, 735–743.
30 C. Graf, D. L. J. Vossen, A. Imhof and A. van Blaaderen, *Langmuir*, 2003, **19**, 6693–6700.

 